analytical chemistry

Article

pubs.acs.org/ac

Workflow for Combined Proteomics and Glycomics Profiling from Histological Tissues

Lilla Turiák,[†] Chun Shao,[†] Le Meng,[†] Kshitij Khatri,[†] Nancy Leymarie,[†] Qi Wang,[†] Harry Pantazopoulos,[‡,§] Deborah R. Leon,[†] and Joseph Zaia*[,†]

[†]Center for Biomedical Mass Spectrometry, Department of Biochemistry, Boston University School of Medicine, Boston, Massachusetts 02118, United States

[‡]Department of Psychiatry, Harvard Medical School, Boston, Massachusetts 02115, United States

[§]Translational Neuroscience Laboratory, McLean Hospital, Belmont, Massachusetts 02478, United States

Supporting Information

ABSTRACT: Extracellular matrixes comprise glycoproteins, glycosaminoglycans and proteoglycans that order the environment through which cells receive signals and communicate. Proteomic and glycomic molecular signatures from tissue surfaces can add diagnostic power to the immunohistochemistry workflows. Acquired in a spatially resolved manner, such proteomic and glycomic information can help characterize disease processes and be easily applied in a clinical setting. Our aim toward obtaining integrated omics datasets was to develop the first workflow applicable for simultaneous analysis of glycosaminoglycans, *N*-glycans and proteins/peptides from tissue surface areas as small as 1.5 mm in diameter. Targeting small areas is especially important in the case of glycans, as their distribution can be very heterogeneous between different tissue regions. We first established reliable and reproducible digestion protocols for the individual compound classes by applying standards on the tissue using microwave irradiation to achieve reduced digestion times. Next, we developed a multienzyme workflow suitable for analysis of the different compound classes. Applicability of the workflow was demonstrated on serial mouse brain and liver sections, both fresh frozen and formalin-fixed. The glycomics data from the 1.5 mm diameter tissue surface area was consistent with data published on bulk mouse liver and brain tissues, which demonstrates the power of the workflow in obtaining combined molecular signatures from very small tissue regions.

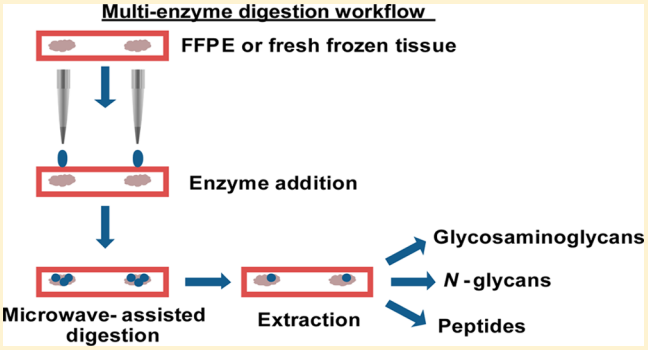

The importance of analysis of discrete tissue regions, rather than bulk tissues, has become clear in the past few years. Direct tissue surface analysis enables detection of localized changes in different compound classes of interest. Matrix-assisted laser desorption/ionization mass spectrometry (MALDI-MS) imaging is used widely for the characterization of spatial and temporal differences in distribution of molecular signatures on histological slides including peptides,[1−3] proteins,[4,5] lipids[6,7] and metabolites.[8,9] However, applying this technique directly to the comparatively labile glycan classes poses several technical challenges, as a permethylation step is necessary to avoid dissociation of sialic acid containing structures. A recent article demonstrated the applicability of direct MALDI-MS imaging for native *N*-glycans in which glycan compositions were validated using parallel analysis of glycans extracted from the surface and then permethylated.[10] The depth of analysis (number of proteins detected and/or identified) is limited for direct MALDI-MS and the signal intensities are influenced by spatially variable effects on the ionization process. This has led to the appearance of alternative methods for analyzing proteolytic peptides recovered from tissue surfaces using liquid-chromatography-mass spectrometry (LC-MS), which produces greater depth of proteomics coverage concerning less abundant proteins.[11−13]

Electrospray-based methods for tissue analysis have focused in two directions; the first is dissection of tissue followed by conventional bottom-up proteomics workflows.[13−16] The advantage of this approach is that it uses straightforward solution-based proteomics, in contrast to the more challenging option where enzymatic digestion is performed on the tissue surface itself.[11,12] The second, direct nanoelectrospray ionization of tissue surfaces, is possible using ambient ionization techniques including desorption electrospray ionization (DESI).[17] This method allows rapid and direct analysis of tissue sections without the need for time-consuming sample preparation. Microextraction using a liquid extraction surface analysis (LESA) interface[18] has been applied to both fresh

Received: June 16, 2014
Accepted: September 9, 2014
Published: September 9, 2014

   dx.doi.org/10.1021/ac5022216 | *Anal. Chem.* 2014, 86, 9670−9678

frozen[11] and formalin fixed paraffin embedded (FFPE)[12] tissues. In our experience, however, use of LC-MS favors reproducible results[19] due to the LC step, which removes lipids and other molecules on the tissue surface. In the absence of the LC step, ionization of biomolecules varies spatially due to the presence of surface effects.

Analysis of glycans from tissue surfaces has been previously demonstrated for *N*-glycans,[20,21] *O*-glycans,[21] and glycosaminoglycans (GAGs).[22−25,19] Similar to proteins, *N*-glycans can be analyzed by LC-MS following on-surface enzymatic digestion and extraction. This has been demonstrated on model glycoproteins, human blood serum and mouse brain tissue following reduction and permethylation.[20] Our group has recently developed a digestion protocol for GAGs and shown its applicability for heparan sulfate (HS) from fresh frozen bovine brain tissues with a 5 × 5 mm spot size.[19] Usefulness of the method was demonstrated on human astrocytoma (WHO grade II) and glioblastoma (WHO grade IV) slides where significant differences were detected in HS disaccharide abundances.

Our aim in the present study was to develop a workflow for analysis of compound classes including GAGs, *N*-glycans and proteins from the same tissue target. To achieve these results, it was necessary to optimize conditions of the workflow separately for each compound class. Analysis of both proteins and multiple glycan classes from the same tissue surface spot has not been reported previously. Identification of different molecular signatures from the very same tissue area increases the information content and has an added value as opposed to analyzing only one compound class. This workflow enables simultaneous characterization of changes in different molecules in case of diverse disease processes. GAGs are linear polysaccharides that play pivotal roles in several biological processes through protein binding[26] and have been found to be associated with pathological diseases.[27−29] They are present in extracellular matrix, intracellular granules and cell surfaces. *N*-glycosylation influences processes including systemic immune response,[30] tumor growth and metastasis.[31] Our rationale was that profiling of different glycan classes and proteins would yield more detailed information regarding the spatially and temporally regulated tissue phenotypes in pathological conditions. We demonstrate a workflow for analysis of multiple glycan classes and proteins from single tissue spots. Biological reproducibility will be the subject of future studies that use the methods described here.

EXPERIMENTAL SECTION

Materials. Fresh frozen bovine cerebral cortex slides containing two 15 μm thick sections, FFPE bovine cerebral cortex slides (5 μm thick, 4 sections per slide) and fresh frozen mouse caudate putamen brain coronal sections (10 μm) were purchased from Zyagen (San Diego, CA). RapiGest SF was obtained from Waters (Milford, MA). Hyaluronidase was obtained from Seikagaku America/Associates of Cape Cod (Falmouth, MA). Mass spectrometry grade trypsin was purchased from Promega (Madison, WI). Heparin lyases II and III were generous gifts from Prof. Jian Liu (UNC Eshelman School of Pharmacy, Chapel Hill, NC). PNGase F and heparin lyase I were obtained from New England Biolabs (Andover, MA); all other reagents including GAG and *N*-glycan standards were from Sigma-Aldrich (St. Louis, MO).

Digestion of Standards Spiked on Tissue. Five cycles of 0.5 μL chondroitinase ABC (1 milliunits/μL), PNGase F (100,000 units/mL) or trypsin (100 ng/μL) enzyme solution were applied manually on predetermined spots of bovine cortex tissue slides spiked with standards (250 ng chondroitin sulfate A, 10 μg ribonuclease B (RNaseB), 10 μg transferrin (TRFE) or 1 μg transferrin). During the cycles, slides were either irradiated using a domestic microwave for 10 min at 270 W or placed in an incubator at 37 °C for 40 min. To circumvent rapid evaporation of the enzyme digestion solutions from tissue surfaces, the whole digestion process was performed in a humidified box for incubator incubation and humidified Petri dishes for microwave irradiation. Enzymes were applied in multiple cycles. Chondroitinase ABC enzyme solution contained 5 mM Tris−HCl pH 8.0 and 2.5 mM ammonium acetate. PNGase F and trypsin stock solutions were diluted in 50 mM ammonium bicarbonate. Before the trypsin enzyme solution was applied, the digestion spots were first reduced and alkylated as follows. First, 0.5 μL of a solution containing 10 mM DTT, 0.1% RapiGest and 10% glycerol was applied on the chosen spots and the tissue slide was incubated at 55 °C for 20 min. Next, 0.5 μL of a solution containing 20 mM iodoacetamide, 25 mM ammonium bicarbonate and 10% glycerol was added and the tissue slide placed in a darkbox for 20 min at room temperature. This was followed by the addition of the trypsin enzyme solution in the presence of 10% glycerol. Following digestion, the resulting CS disaccharides, *N*-glycans or peptides were extracted manually by 1 μL 0.3% ammonium hydroxide solution, water and 10% acetic acid, respectively. Extraction was repeated four times for each digestion spot and the extracts were combined. Subsequent LC-MS methods and data interpretation can be found in the Supporting Information.

Digestion of Tissues Spots. Aligned digestion spots were chosen on six serial sections of both fresh frozen and fixed mouse liver and mouse caudate putamen slides (each 10 μm thick). First, five cycles of hyaluronidase enzyme solution (0.16 TRU/μL hyaluronidase in the presence of 2 M ammonium acetate and 10% glycerol) was applied on the chosen spots. The resulting HA disaccharides were extracted four times by 0.3% ammonium hydroxide solution and the slides were dried at 55 °C for 5 min, which was followed by 20 min incubation at 37 °C with 50 mM ammonium bicarbonate. Next, five cycles of chondroitinase ABC (1 milliunits/μL) enzyme solution was added. To minimize the amount of salt in the enzyme solution, the 5 mM Tris buffer was replaced by 25 mM ammonium bicarbonate buffer and 10% glycerol was also added to minimize diffusion. The resulting CS disaccharides were extracted as the HA disaccharides and the slide was dried at 55 °C for 5 min, which was followed by 20 min incubation with 25 mM ammonium bicarbonate at 37 °C. Next, five cycles of heparin lyase I, II and III mixture was added. The solution contained 1.66 mU/μL of heparin lyase I, 0.33 mU/μL of herparin lyase II and 0.33 mU/μL of heparin lyase III in the presence of 2.5 mM calcium hydroxide, 12.5 mM ammonium bicarbonate and 10% glycerol. The resulting HS disaccharides were extracted as the HA and CS disaccharides and the slide was dried at 55 °C for 5 min, which was followed by 20 min incubation with 50 mM ammonium bicarbonate at 37 °C. Next, a solution containing 10 mM DTT, 0.1% RapiGest and 10% glycerol was applied on the chosen spots and the tissue slide was incubated at 55 °C for 20 min. This was followed by addition of a solution containing 20 mM iodoacetamide, 25 mM ammonium bicarbonate and 10% glycerol and the tissue slide was placed in a darkbox for 20 min at room temperature.

dx.doi.org/10.1021/ac5022216 | Anal. Chem. 2014, 86, 9670−9678

Next, five cycles of trypsin enzyme solution (100 ng/μL) in the presence of 10% glycerol were added to achieve digestion of proteins. Samples were then incubated with aprotinin (2 μg/μL) at 37 °C for 45 min to stop trypsin activity. Finally, five cycles of PNGase F (500,000 units/mL) were added. The peptides and glycans were extracted by 10% acetic acid and separated by C18 spin column. Samples were loaded in 5% ACN/0.1%FA, the flow-through and wash fraction contained the *N*-glycans, while peptides were released first by 40% ACN 0.1% FA then by 60% ACN 0.1% FA, combined and dried under vacuum. Individual cycles consisted of microwave irradiation for 10 min (for CS, HS and proteins, 270 W; for HA, 540 W) except for *N*-glycans where incubation took place in an incubator (37 °C, 40 min/cycle). Subsequent LC-MS methods and data interpretation can be found in the Supporting Information along with a table summarizing the experiments performed (Table S-1, Supporting Information).

RESULTS AND DISCUSSION

As a first step, we optimized digestion conditions separately for each compound class applying standards to both fresh frozen and FFPE bovine brain cortex sections. After optimizing conditions for microwave-assisted digestion, we developed a multienzyme workflow for consecutive digestion of GAGs, *N*-glycans and proteins on 1.5 mm diameter tissue surface areas of both fresh frozen and fixed mouse liver and brain sections for subsequent LC-MS analysis (Figure 1).

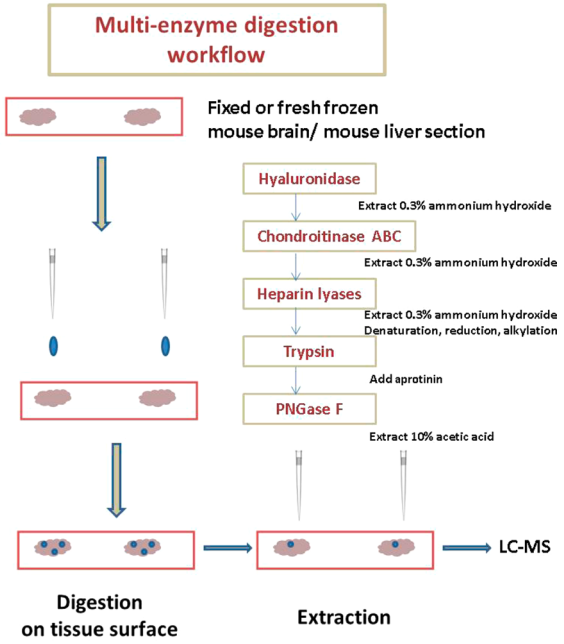

Figure 1. Diagram summarizing the developed multienzyme workflow.

Optimizing Microwave-Assisted on Tissue Digestion for GAGs. We compared digestion in an incubator versus microwave irradiation with the goal of minimizing tissue surface glycosidase digestion times. Chondroitin sulfate A (CS-A) was used for method development. The initial results regarding the use of microwave-assisted digestion indicated that care must be taken to balance microwave power and digestion time in order to achieve efficient, reproducible glycosidase digestion of GAGs on tissue surfaces. Five cycles of 0.5 μL Chondroitinase ABC enzyme solution were applied on areas of a fresh frozen bovine brain cortex slide spiked with 0.5 μL 250 ng CS-A as a standard. Time of incubation was 40 min/cycle for incubator and 10 min/cycle for microwave incubation. Disaccharides were extracted as described previously,[19] using 0.3% ammonium hydroxide solution. The normalized extracted ion chromatogram of the most abundant singly sulfated disaccharide (m/z 458, D0a4/D0a6) in the SEC-MS run was very similar in the case of five cycles of digestion in an incubator versus five cycles of microwave-assisted digestion (Figure 2a). The same was observed for the less abundant nonsulfated disaccharide (m/z 378, D0a0) as well (Figure 2a). The CS disaccharide nomenclature is described in Figure 2. The amount of enzyme added in each cycle was the same for both incubation types (1 milliunit/μL). These results indicate that digestion time can be significantly reduced from 200 to 50 min by using microwave-assisted digestion for GAGs. Variation in number of cycles was compared using both microwave and incubator enzyme digestion. Similar signal intensities could be observed in case of both digestion types on unspiked tissue (Figure S-1, Supporting Information) when using the same incubation time. The optimum number of cycles was determined using CS-A standard in the case of the microwave incubation. Digestion products were extracted after 1, 3, 5 and 7 cycle enzyme addition. As expected, the normalized extracted ion chromatogram of the singly sulfated disaccharide increases with the increasing number of cycles (Figure S-2a, Supporting Information). For CS, the low abundance nonsulfated disaccharide (D0a0) was detected only after 5 cycles of enzyme addition. Recovery of the disaccharides was also tested when the standard was applied on FFPE tissue (Figure S-3a, Supporting Information). Results showed that nearly twice as much CS disaccharide was recovered from fresh frozen tissues as opposed to FFPE (Figure S-3a, Supporting Information). After microwave-assisted digestion conditions for exogenous chondroitin sulfate (CS) standard were optimized, areas of unspiked fresh frozen bovine brain cortex samples were analyzed. Two spot sizes (0.5 μL corresponding to 1 mm and 1 μL corresponding to 1.5 mm diameter tissue surface) were compared with two replicates for each. The relative abundances of the singly sulfated (D0A4/D0a6) (69% for 0.5 μL and 65% for 1 μL spot size) and nonsulfated (D0A0) (31% for 0.5 μL and 35% for 1 μL spot size) disaccharides were independent from the spot size analyzed and signal intensities were higher in the case of the larger spot (Figure S-4a, Supporting Information). These experiments confirmed that microwave-assisted tissue surface digestion of GAGs may be achieved from target diameters as small as 1 mm (0.5 μL spot size). Furthermore, the coefficients of variation (cv) were less than 10% for the detected disaccharides for the 0.5 μL spot size.

Optimizing Microwave-Assisted on Tissue Digestion for *N*-Glycans. In the case of *N*-glycans, two standard glycoproteins were selected for method optimization; Ribonuclease B (RNase B), which displays high mannose type *N*-glycans,[32] and serotransferrin (TRFE), which contains complex type *N*-glycans.[33] Quantities of 10 μg of the standard glycoproteins were spiked on tissue sections and dried. The enzymatically released *N*-glycans were extracted using water. Native *N*-glycans were analyzed using hydrophilic interaction chromatography (HILIC)-MS in the negative ion mode, under which conditions dissociation of sialic acid containing glycans is minimized. High mannose *N*-glycans released from 10 μg RNase B added exogenously to a fresh frozen bovine cortex slide gave higher signal intensities using an incubator than for

dx.doi.org/10.1021/ac5022216 | Anal. Chem. 2014, 86, 9670−9678

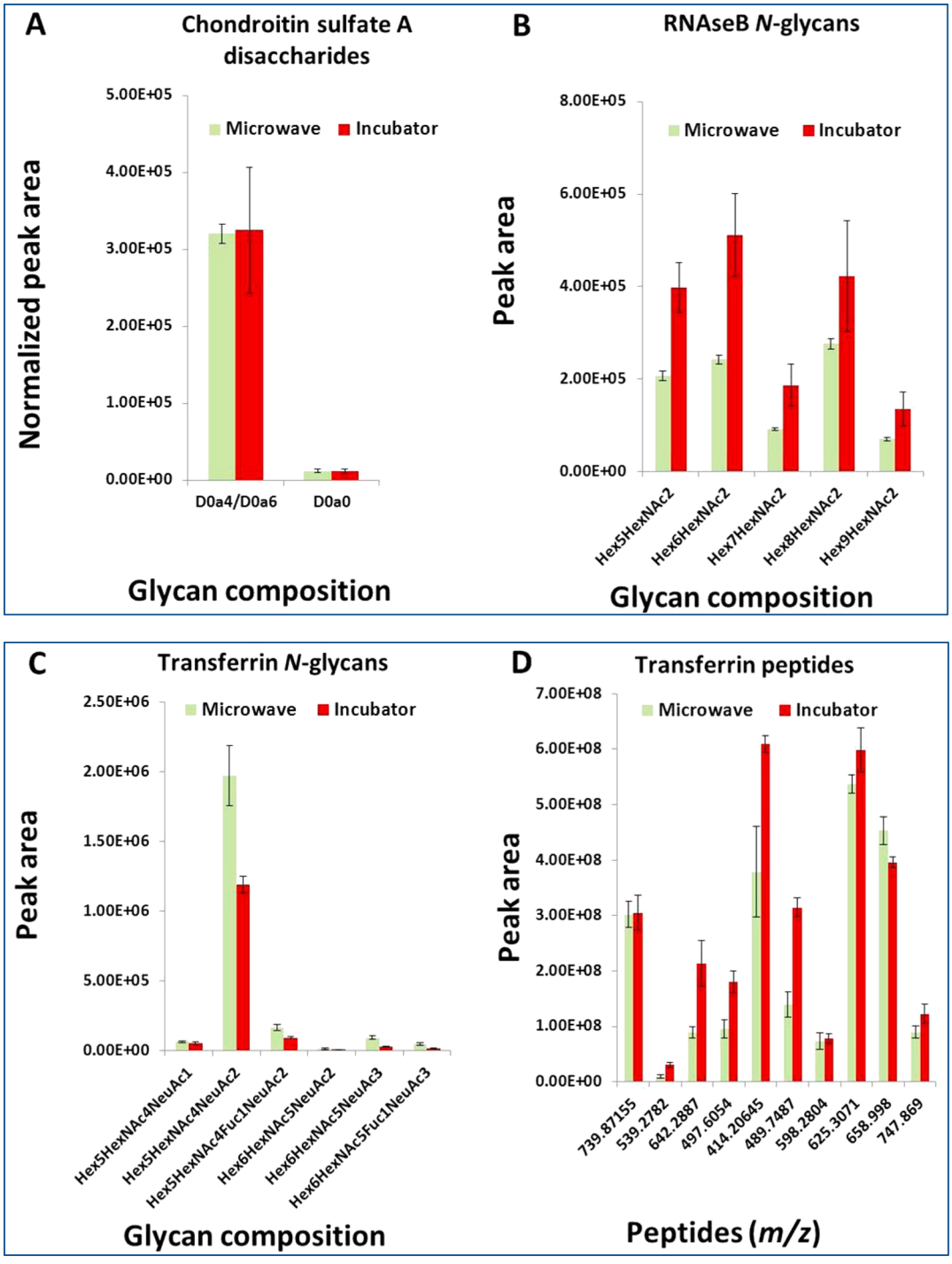

Figure 2. Comparison of microwave-assisted and conventional digestion for five cycles of enzyme addition on three serial fresh frozen bovine brain cerebral cortex sections spiked with internal standards and digested by different enzymes, (A) chrondroitin sulfate A (250 ng), (B) RNase B (10 μg), (C) TRFE (10 μg) and (D) TRFE (1 μg). CS disaccharide abundances of CS-A standard (A), native *N*-glycan abundances of RNase B standard (B), native *N*-glycan abundances of TRFE standard (C) and peptide abundances of TRFE standard (D). The *m*/*z* values correspond to the following peptides: 739.87155 (K.MYLGYEYVTAIR), 539.2782 (K.HSTIFENLANKADR), 642.2887 (K.EGYYGYTGAFR), 497.6054 (K.DLLFKDSAHGFLK), 414.20645 (K.NPDPWAK), 489.7487 (K.DGAGDVAFVK), 598. 2804 (K.DSGFQMNQLR), 625.3071 (K.SASDLTWDNLK), 658.998 (K.HQTVPQNTGGKNPDPWAK) and 747.869 (K.MYLGYEYVTAIR.N + Oxidation (M)). Error bars show the standard error. The following nomenclature is used for the CS disaccharides.[45] The unsaturated uronic acid is marked by a "D", whereas the galactosamine is marked by an "a". The number after "D" denotes the nonreducing end *O*-sulfation (0 if it is nonsulfated and 2 if it is 2-*O*-sulfated), whereas the number after "a" denotes hexosamine *O*-sulfation (0 if it is nonsulfated, 4 if it is 4-*O*-sulfated and 6 if it is 6-*O*-sulfated). The following abbreviations are used for *N*-glycan nomenclature Hex = hexose, HexNAc = hexosamine, Fuc = deoxyhexose, NeuAc = *N*-acetylneuraminic acid, NeuGc = *N*-glycolylneuraminic acid.

microwave-assisted digestion (Figure 2b). However, for the larger TRFE glycoprotein, microwave irradiation yielded higher signal intensities for the complex-type native *N*-glycans (Figure 2c). Nomenclature of *N*-glycans is described in Figure 2. The

dx.doi.org/10.1021/ac5022216 | *Anal. Chem.* 2014, 86, 9670−9678

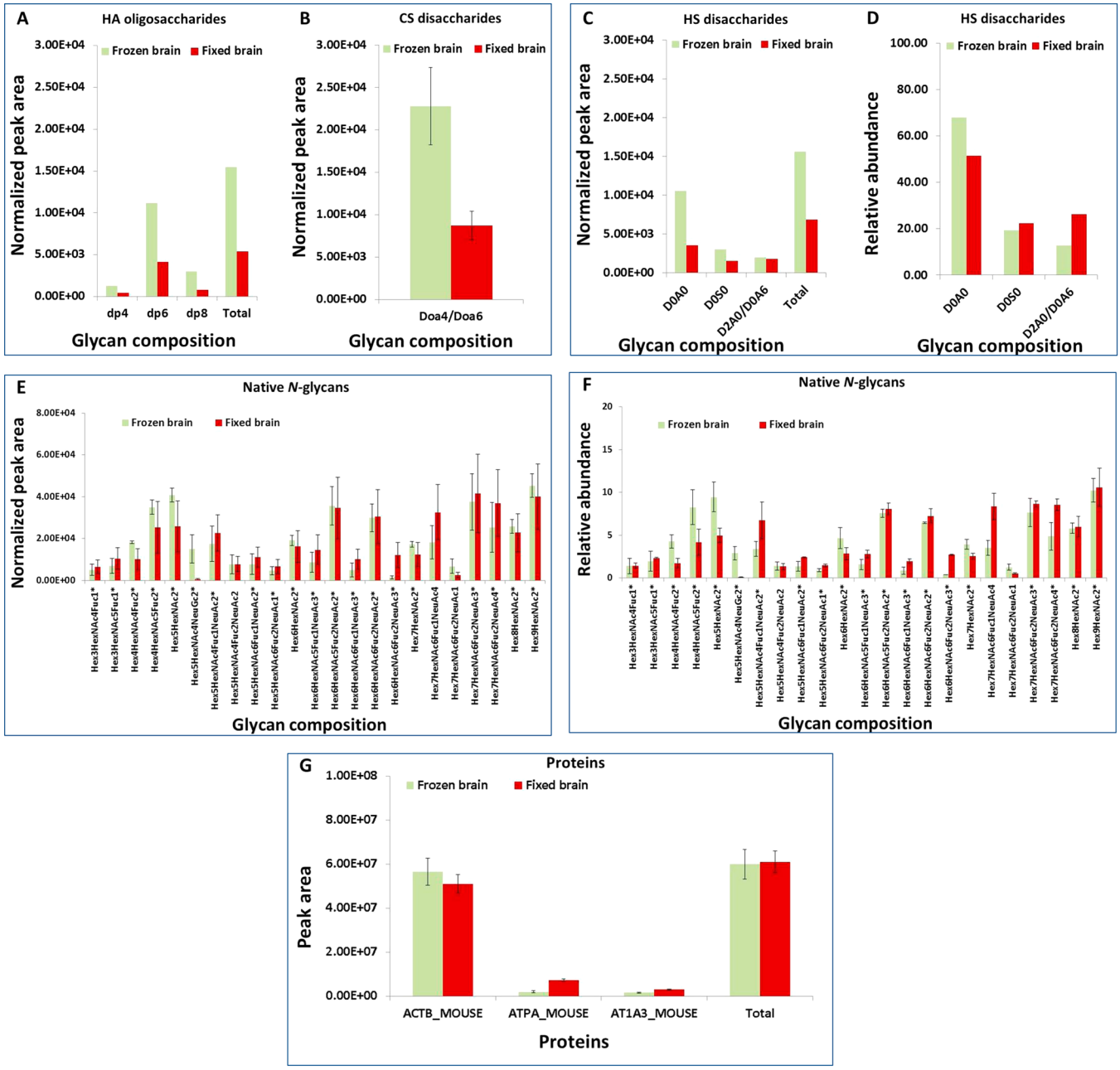

Figure 3. Consecutive enzyme digestion to fresh frozen and fixed mouse brain tissues. Abundances of HA depolymerization products (A), abundances of CS disaccharides (B), abundances of HS disaccharides (C,D), absolute abundances of native *N*-glycans (E), relative abundances of native *N*-glycans (F) and abundances of ACTB_MOUSE, ATPA_MOUSE and AT1A3_MOUSE proteins (G). Panel C shows HS disaccharide abundance normalized to internal standard and protein content, whereas panel D represents the % abundance of the disaccharide structures normalized to the summed intensity of all disaccharide structures of the sample. Error bars show the standard error where applicable. Hyaluronic acid depolymerization products (A) and heparan sulfate disaccharides (C and D) could only be detected in the combined extracts of serial sections in mouse brain samples; therefore there are no error bars in case of these samples. Panels E and F represent results of three triplicate measurements of the combined *N*-glycan extracts of serial sections. The following nomenclature is used for the HS disaccharides.[45] The unsaturated uronic acid is marked by a "D", whereas the glucosamine is marked by an "A" if it is unsulfated and by an "S" if it is *N*-sulfated. The number after "D" denotes the nonreducing end *O*-sulfation (0 if it is nonsulfated and 2 if it is 2-*O*-sulfated), while the number after "A" or "S" denotes hexosamine *O*-sulfation (0 if it is nonsulfated and 6 if it is 6-*O*-sulfated).

optimum number of cycles for microwave irradiation was found to be five; an increase to 7 cycles reduced signal intensities to a value similar to digestion in an incubator (Figure S-2b, Supporting Information). On-tissue glycan release of TRFE gave similar native *N*-glycan distribution profiles as previously reported.[34] The doubly sialylated biantennary and doubly sialylated biantennary structures with one fucose account for nearly 90% of glycosylation.

During method development, different sample cleanup methods were compared to maximize recovery of sialylated glycans. A 10 μg quantity of TRFE was applied on a glass slide and after digestion cleaned up using HILIC ultramicrospin columns, HILIC tips or PGC tips. Three replicates were

dx.doi.org/10.1021/ac5022216 | *Anal. Chem.* 2014, 86, 9670−9678

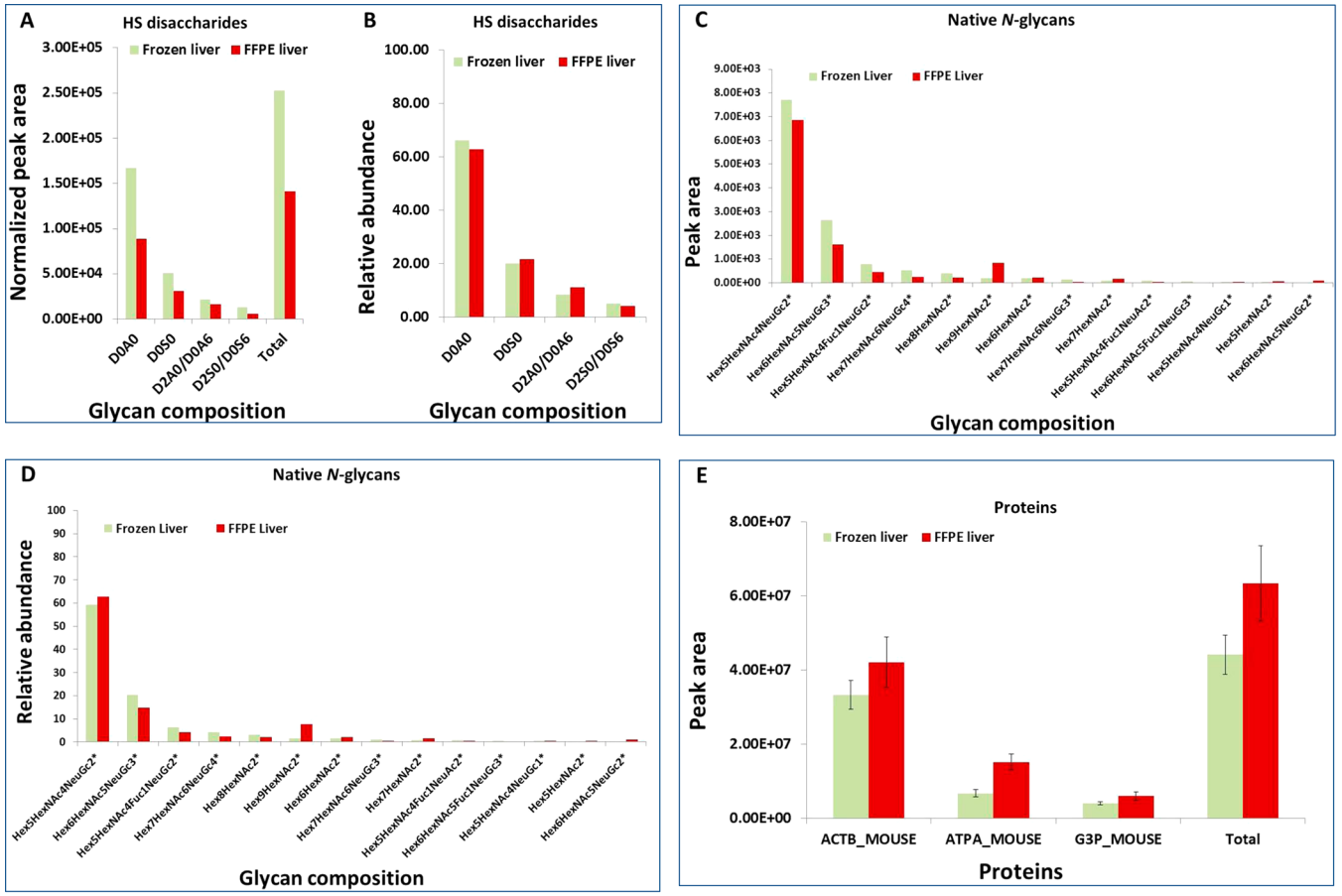

Figure 4. Consecutive enzyme digestion to fresh frozen and FFPE mouse liver tissues. Abundances of HS disaccharides (A,B), absolute abundances of native *N*-glycans (C), relative abundances of native *N*-glycans (D) and abundances of ACTB_MOUSE, ATPA_MOUSE and G3P_MOUSE proteins (E). Panel A shows HS disaccharide abundance normalized to internal standard and protein content, whereas panel B represents the % abundance of the disaccharide structures normalized to the summed intensity of all disaccharide structures of the sample. The error bars show the standard error where applicable. Heparan sulfate disaccharides (A,B) and native *N*-glycans (C,D) could only be detected in the combined extracts of serial sections in mouse liver samples; therefore, there are no error bars in the case of these samples.

performed in each case. Highest intensities were observed for the PGC tip in the case of each detected glycan (Figure S-5, Supporting Information). For the remainder of the experiments, this sample cleanup method was used. Recovery of *N*-glycans was compared both for standards spiked on fresh frozen tissues and FFPE tissues (Figure S-3b and S-3c, Supporting Information). No significant differences were observed whether standards were spiked on fresh frozen or FFPE tissue. Analysis of *N*-glycans from unspiked tissue slides posed a greater challenge; native *N*-glycans from unspiked samples could only be detected if incubation time and spot size were increased (see results below).

Optimizing Microwave-Assisted on Tissue Digestion for Proteins/Peptides. We optimized conditions for reproducible recovery of peptides from the histological surface while minimizing dispersion during the denaturation, reduction, alkylation and enzymatic digestion steps. We found that adding 10% glycerol to each reaction solution minimized dispersion by maintaining sufficient surface tension necessary for well-defined tissue surface droplets. The glycerol was washed away during sample cleanup and did not adversely impact the subsequent LC-MS analysis. We also observed significantly less dispersion using 10% acetic acid extraction solution rather than the conventionally used 80% ACN, 0.1% formic acid solution. Regarding the sample cleanup method, we found C18 spin columns to produce more reproducible results than C18 ZipTips (Figure S-6, Supporting Information). To test reproducibility, the fresh frozen and FFPE samples were spiked with 1 μg of TRFE. A total of 10 transferrin peptides were selected and the areas of the extracted ion chromatograms were compared both for incubator and microwave incubation. With the exception of one peptide, digestion in an incubator gave higher signal intensities (Figure 2d). Increasing the number of cycles of microwave irradiation to seven reduced the observed signal (Figure S-2d, Supporting Information). Recovery of TRFE peptides from FFPE was lower than from fresh frozen slides (Figure S-3d, Supporting Information). The total number of proteins identified from three replicates was very similar, independent of the tissue type (fresh frozen or FFPE) both for digestion in the microwave oven and incubator (Figure S-7, Supporting Information). More than 70% of the proteins detected were identified in both sample types (Figure S-7a and S-7b, Supporting Information). During initial method development, different types of denaturants were also tested. In terms of number of proteins identified, RapiGest worked better than 2,2,2,-trifluoroethanol (TFE) (data not shown).

Applicability of Microwave-Assisted on Tissue Digestion for Multiple Compound Classes. After digestion conditions were optimized individually for each compound class, consecutive enzyme digestion and simultaneous analysis

dx.doi.org/10.1021/ac5022216 | *Anal. Chem.* 2014, 86, 9670−9678

of different compound classes from a given spot became feasible. This was demonstrated on serial sections of fresh frozen and fixed slides from mouse brain and liver, respectively. The workflow consisted of addition of GAG degrading enzymes (hyaluronidase, chondroitinase ABC and heparin lyases), trypsin and PNGase F, in series. For most GAG disaccharide and *N*-glycan samples, combining the extraction products of the serial sections was necessary to obtain acceptable mass spectrometry signal intensity. The GAG and *N*-glycan abundances were normalized with respect to protein abundances from the same tissue in the following way: 5 peptides of three proteins present in each mouse liver and brain samples were chosen and the peak areas for these 15 peptides were determined and data normalized to the summed intensity. Depolymerized GAGs were analyzed using SEC-MS in the negative ion mode, where the limit of detection is approximately 1 pmol for disaccharides. Hyaluronic acid depolymerization products could only be detected in the combined mouse brain samples and not in combined liver samples. This is not surprising as it has been reported for various species that hyaluronan (HA) expression in liver is much lower than in brain, kidney or lung.[35] The detected HA saccharides in mouse brain corresponded to degree of polymerization (dp) 4, dp 6 and dp 8, both detected in higher intensities from frozen tissue (Figure 3a). CS expression was high in the brain[36] and we were able to detect CS disaccharides from all six replicates from fresh frozen and fixed slides (Figure 3b). The normalized abundance of the singly sulfated disaccharide was nearly three times higher for fresh frozen brain tissue than fixed (Figure 3b).

CS disaccharides originating from the liver could not be identified with our current disaccharide analysis method, not even when the samples from the serial sections were combined. Concentration of CS and HA in rat liver microsomes is about 5−10% respective to brain microsomes,[37] which may explain why neither CS disaccharides nor HA depolymerization products from mouse liver could be detected. Heparan sulfate (HS) disaccharides were detected both in the combined mouse liver (Figure 4a,b) and brain samples (Figure 3c,d). Nomenclature for HS disaccharides can be found in Figure 3. There is good agreement in the literature that the most abundant HS structure both in brain and liver mouse tissue is the nonsulfated disaccharide, accounting for roughly 50% of all HS disaccharides.[38−40] We also found the nonsulfated disaccharide to be the most abundant (Figures 3d, 4b). As opposed to the literature, we did not detect any trisulfated structures; most probably these were present under the limit of detection of the SEC-MS method used in these studies.

Released *N*-glycans were detected after pooling six replicates of each sample. A significant difference in the *N*-glycans present in mouse liver and brain tissue is in the terminal sialic acid. We detected many NeuGc containing *N*-glycan compositions in liver samples (Figure 4c,d). In total, 13 *N*-glycan compositions were detected from fresh frozen and 14 from FFPE liver (Table S-2, Supporting Information). The glycan compositions can be found in Figure 4c,d. Most of the identified *N*-glycan compositions have been reported by either the Consortium for Functional Glycomics (http://www.functionalglycomics.org) or by Lee et al.[41] These compositions are marked by an asterisk in the figure. We observed that the most abundant *N*-glycan composition in the liver samples, accounting for over 50% of the total, is the biantennary bisialylated composition $Hex_5HexNAc_4NeuGc_2$. High mannose glycan compositions $Hex_6HexNAc_2$ and $Hex_9HexNAc_2$ were also among the more abundant constituents (Figure 4c,d). Brain samples were more complex, as 45 *N*-glycan compositions were detected in fresh frozen and 47 in fixed samples. This number is very similar to that reported by Mechref et al.[20] using off-tissue permethylation. More than 70% of the identified brain *N*-glycan compositions contained at least one fucose residue. According to preliminary experiments performed on mouse brain slides we found that the *N*-glycan distribution within the brain is very heterogeneous. Therefore, we focused on adding the enzyme to a relatively homogeneous area, the primary motor cortex (M1), consisting of cortical layers 2 through 6 (Figure S-8, Supporting Information). Cortical layer I was avoided due to the established high concentration of glial cells and lack of neurons in this layer. Figure 3e,f shows the absolute and relative ion abundances of glycans, which are present in either sample over 1% of the total ion abundance. The complete list of the *N*-glycan compositions identified from triplicate measurements of combined brain samples can be found in the Supporting Information (Table S-3).

The total number of proteins identified for the six replicates was the following: 100 for frozen brain, 92 for fixed brain, 62 for frozen liver and 74 for FFPE liver. The relatively low number of proteins identified can be explained by the size of the tissue area analyzed. Wisztorski et al.[12] analyzed similar digestion areas and identified approximately 10-fold more proteins. Our results contain proteins only if they were identified by at least two unique peptides. Accepting proteins with one unique peptide would double the amount of proteins identified in our study. The list of identified proteins can be found in the Supporting Information (Tables S-4 and S-5). Proteomics results obtained from the surface of the primary motor cortex area of the brain were compared with a recent article analyzing normal dissected murine brain regions.[42] A total of 60% of the proteins identified from fresh frozen and 50% of the proteins identified from fixed tissue surfaces were found among those for the dissected brain regions. The majority of the proteins that were not detected in this previous study were membrane proteins (e.g., THY1_MOUSE, MOG_MOUSE, MYPR_MOUSE, etc.). Other examples were nucleolar proteins (e.g., histones, RL6_MOUSE, ROA1_MOUSE, etc.). The high amount of membrane proteins detected from the tissue surface is also a significant advantage of our workflow. Liver samples were rich in enzymes; carbamoyl-phosphate synthase and albumin proteins produced the largest number of identified peptides. Among the identified proteins, 90% have been described previously by one of two major liver proteome studies.[43,44]

Normalizing to the tissue surface area digested is relatively straightforward; however, our aim was to compare the glycan signatures among the different samples and decided to normalize our data to housekeeping tissue proteins in the sample, the expression of which are constant. All glycomics data was normalized to proteins of the respective tissue the following way: five peptides of three housekeeping proteins were chosen for data normalization. ACTB_MOUSE, ATPA_MOUSE and AT1A3_MOUSE proteins were used in case of mouse brain and ACTB_MOUSE, ATPA_MOUSE and G3P_MOUSE proteins in case of mouse liver tissues. The glycomics data were normalized to the total intensity of these three proteins. Figures 3g and 4e show the amount of the three selected proteins ACTB_MOUSE (m/z 488.7278 AGFAGDDAPR, m/z 400.2400 AVFPSIVGRPR, m/z 652.0263

dx.doi.org/10.1021/ac5022216 | *Anal. Chem.* 2014, 86, 9670−9678

VAPEEHPVLLTEAPLNPK, *m/z* 895.9496 SYELPDGQVITIGNER and *m/z* 581.3137 EITALAPSTMK), ATPA_MOUSE (*m/z* 712.3403 TGTAEMSSILEER, *m/z* 788.3966 ILGADTSVDLEETGR, *m/z* 812.9488 TGAIVDVPVGEELLGR, *m/z* 374.2449 VGLKAPGIIPR and *m/z* 513.8007 AVDSLVPIGR), AT1A3_MOUSE (*m/z* 520.7904 GGQDNIPVLK, *m/z* 638.3500 DVAGDASESALLK, *m/z* 610.3195 VAEIPFNSTNK, *m/z* 610.6461 GVGIISEGNETVEDIAAR and *m/z* 604.6547 QGAIVAVTGDGVNDSPALK) and G3P_MOUSE (*m/z* 764.3560 WGEAGAEYVVESTGVFTTMEK, *m/z* 685.3753 GAAQNIIPASTGAAK, *m/z* 398.2127 LTGMAFR, *m/z* 890.4023 LISWYDNEYGYSNR and *m/z* 678.8305 VVDLMAYMASKE) and their total in the different samples. The average coefficients of variation for the 15 peptides among the different samples are the following: 27.7% for frozen brain, 19.4% for fixed brain, 30.9% for frozen liver and 40.8% for FFPE liver. These results reflect both biological and analytical reproducibility derived from biological material and a complex workflow and therefore can be considered acceptable. The results for different compound classes summarized in Figures 3 and 4 demonstrate the applicability of the workflow for obtaining combined glycomics and proteomics information when analyzing very small tissue areas.

We found that microwave irradiation significantly accelerated the digestion process when compared to incubator incubation in the case of standards applied to the tissue surface. Equivalent results were achieved using frozen or fixed tissue. It was of special importance to demonstrate that the workflow allows analysis of compounds from target areas smaller than 2 mm in diameter, as it can be a very powerful tool for tissue microarray analysis. Achieving reproducible results was the major concern and therefore received the most attention. Reagent concentrations were kept similar to conditions typically used for in-solution digestion. To avoid rapid evaporation of the enzyme digestion solutions, the whole digestion process was performed under humidified conditions and enzymes were applied in multiple cycles. Dispersion of the enzyme droplets was minimized by adding 10% glycerol to each reaction solution. Glycerol helps maintain sufficient surface tension resulting in well-defined tissue surface droplets. For method development and optimization purposes standards were applied on commercially available fresh frozen and FFPE bovine cerebral cortex sections. In the case of the multienzyme workflow, in-house prepared mouse liver and commercial mouse brain tissues were used, as a way of demonstrating the usefulness of the workflow in detecting differences in molecular signatures between various tissue types.

CONCLUSIONS

A useful and efficient microwave-assisted multienzyme digestion workflow was developed for combined proteomics and glycomics from tissue surfaces. GAG degrading enzymes, trypsin and PNGase F were sequentially added to the same area of interest and the digestion products were analyzed using LC-MS. The primary advantage of this workflow is that specific areas of a tissue section can be analyzed rather than bulk tissue analysis where the sample is heterogeneous. This method will enable comparison of pathological and nonpathological regions of a given sample. This workflow will be applicable to sample sets such as tissue microarrays and a complementary technique to LCM, which is generally followed by in solution digestion of different compound classes.

ASSOCIATED CONTENT

Supporting Information

Additional information as noted in the text. This material is available free of charge via the Internet at http://pubs.acs.org.

AUTHOR INFORMATION

Corresponding Author

*Joseph Zaia. Address: Boston University Medical Campus, 670 Albany Street, Room 509, Boston, MA 02118. Tel.: 617-638-6762. Fax: 617-638-6761. E-mail: jzaia@bu.edu.

Notes

The authors declare no competing financial interest.

ACKNOWLEDGMENTS

This work was funded by NIH grants R01HL098950, P41GM104603 and S10RR020946.

REFERENCES

(1) Chatterji, B.; Pich, A. *Expert Rev. Proteomics* **2013**, *10*, 381−388.
(2) Takai, N.; Tanaka, Y.; Watanabe, A.; Saji, H. *Bioanalysis* **2013**, *5*, 603−612.
(3) Ljungdahl, A.; Hanrieder, J.; Bergquist, J.; Andersson, M. *Methods Mol. Biol.* **2013**, *1023*, 121−36.
(4) Casadonte, R.; Caprioli, R. M. *Nat. Protoc.* **2011**, *6*, 1695−1709.
(5) MacAleese, L.; Stauber, J.; Heeren, R. M. A. *Proteomics* **2009**, *9*, 819−834.
(6) Fülöp, A.; Porada, M. B.; Marsching, C.; Blott, H.; Meyer, B.; Tambe, S.; Sandhoff, R.; Junker, H.-D.; Hopf, C. *Anal. Chem.* **2013**, *85*, 9156−9163.
(7) Ruh, H.; Salonikios, T.; Fuchser, J.; Schwartz, M.; Sticht, C.; Hochheim, C.; Wirnitzer, B.; Gretz, N.; Hopf, C. *J. Lipid Res.* **2013**, *54*, 2785−2794.
(8) Shanta, S. R.; Kim, T. Y.; Hong, J. H.; Lee, J. H.; Shin, C. Y.; Kim, K.-H.; Kim, Y. H.; Kim, S. K.; Kim, K. P. *Analyst* **2012**, *137*, 5757−5762.
(9) Miura, D.; Fujimura, Y.; Wariishi, H. *J. Proteomics* **2012**, *75*, 5052−5060.
(10) Powers, T. W.; Jones, E. E.; Betesh, L. R.; Romano, P. R.; Gao, P.; Copland, J. A.; Mehta, A. S.; Drake, R. R. *Anal. Chem.* **2013**, *85*, 9799−9806.
(11) Quanico, J.; Franck, J.; Dauly, C.; Strupat, K.; Dupuy, J.; Day, R.; Salzet, M.; Fournier, I.; Wisztorski, M. *J. Proteomics* **2013**, *79*, 200−218.
(12) Wisztorski, M.; Fatou, B.; Franck, J.; Desmons, A.; Farre, I.; Leblanc, E.; Fournier, I.; Salzet, M. *Proteomics: Clin. Appl.* **2013**, *7*, 234−240.
(13) Wisniewski, J. R.; Dus, K.; Mann, M. *Proteomics: Clin. Appl.* **2013**, *7*, 225−233.
(14) Braakman, R. B. H.; Tilanus-Linthorst, M. M. A.; Liu, N. Q.; Stingl, C.; Dekker, L. J. M.; Luider, T. M.; Martens, J. W. M.; Foekens, J. A.; Umar, A. *J. Proteomics* **2012**, *75*, 2844−2854.
(15) Hill, J. J.; Tremblay, T.-L.; Pen, A.; Li, J.; Robotham, A. C.; Lenferink, A. E. G.; Wang, E.; O'Connor-McCourt, M.; Kelly, J. F. *J. Proteome Res.* **2011**, *10*, 2479−2493.
(16) Cha, S.; Imielinski, M. B.; Rejtar, T.; Richardson, E. A.; Thakur, D.; Sgroi, D. C.; Karger, B. L. *Mol. Cell. Proteomics* **2010**, *9*, 2529−2544.
(17) Takats, Z.; Wiseman, J. M.; Gologan, B.; Cooks, R. G. *Science* **2004**, *306*, 471−473.
(18) Kertesz, V.; Van Berkel, G. J. *J. Mass Spectrom.* **2010**, *45*, 252−260.
(19) Shao, C.; Shi, X.; Phillips, J. J.; Zaia, J. *Anal. Chem.* **2013**, *85*, 10984−10991.
(20) Hu, Y.; Zhou, S.; Khalil, S. I.; Renteria, C. L.; Mechref, Y. *Anal. Chem.* **2013**, *85*, 4074−4079.

(21) Matsuda, A.; Kuno, A.; Ishida, H.; Kawamoto, T.; Shoda, J.-i.; Hirabayashi, J. *Biochem. Biophys. Res. Commun.* **2008**, *370*, 259−263.
(22) Koshiishi, I.; Horikoshi, E.; Imanari, T. *Anal. Biochem.* **1999**, *267*, 222−226.
(23) Koshiishi, I.; Takenouchi, M.; Imanari, T. *Arch. Biochem. Biophys.* **1999**, *370*, 151−155.
(24) Oguma, T.; Toyoda, H.; Toida, T.; Imanari, T. *Biomed. Chromatogr.* **2001**, *15*, 356−362.
(25) Zhang, Y. T.; Conrad, A. H.; Tasheva, E. S.; An, K.; Corpuz, L. M.; Kariya, Y.; Suzuki, K.; Conrad, G. W. *Invest. Ophthalmol. Visual Sci.* **2005**, *46*, 1604−1614.
(26) Gesslbauer, B.; Theuer, M.; Schweiger, D.; Adage, T.; Kungl, A. J. *Expert Rev. Proteomics* **2013**, *10*, 77−95.
(27) Ariga, T.; Miyatake, T.; Yu, R. K. *J. Neurosci. Res.* **2010**, *88*, 2303−2315.
(28) Berretta, S. *Neuropharmacology* **2012**, *62*, 1584−1597.
(29) Weyers, A.; Yang, B.; Park, J.-H.; Kim, Y.-S.; Kim, S.-M.; Lee, S.-E.; Zhang, F.; Lee, K. B.; Linhardt, R. J. *Glycoconjugate J.* **2013**, *30*, 701−707.
(30) Marth, J. D.; Grewal, P. K. *Nat. Rev. Immun.* **2008**, *8*, 874−887.
(31) Schultz, M. J.; Swindall, A. F.; Bellis, S. L. *Cancer Metastasis Rev.* **2012**, *31*, 501−518.
(32) Liang, C. J.; Yamashita, K.; Kobata, A. *J. Biochem.* **1980**, *88*, 51−58.
(33) Spik, G.; Bayard, B.; Fournet, B.; Strecker, G.; Bouquelet, S.; Montreuil, J. *FEBS Lett.* **1975**, *50*, 296−299.
(34) Wada, Y.; Azadi, P.; Costello, C. E.; Dell, A.; Dwek, R. A.; Geyer, H.; Geyer, R.; Kakehi, K.; Karlsson, N. G.; Kato, K.; Kawasaki, N.; Khoo, K.-H.; Kim, S.; Kondo, A.; Lattova, E.; Mechref, Y.; Miyoshi, E.; Nakamura, K.; Narimatsu, H.; Novotny, M. V.; Packer, N. H.; Perreault, H.; Peter-Katalinic, J.; Pohlentz, G.; Reinhold, V. N.; Rudd, P. M.; Suzuki, A.; Taniguchi, N. *Glycobiology* **2007**, *17*, 411−422.
(35) Fraser, J. R. E.; Laurent, T. C.; Laurent, U. B. G. *J. Intern Med.* **1997**, *242*, 27−33.
(36) Kwok, J. C. F.; Warren, P.; Fawcett, J. W. *Int. J. Biochem. Cell Biol.* **2012**, *44*, 582−586.
(37) Margolis, R. U.; Margolis, R. K. In *Heparin: Structure, Cellular Functions, and Clinical Applications*; McDuffie, N. M.; Ed.; Academic Press: New York, 1979; pp 227−241.
(38) Ledin, J.; Staatz, W.; Li, J. P.; Gotte, M.; Selleck, S.; Kjellen, L.; Spillmann, D. *J. Biol. Chem.* **2004**, *279*, 42732−42741.
(39) Nagamine, S.; Tamba, M.; Ishimine, H.; Araki, K.; Shiomi, K.; Okada, T.; Ohto, T.; Kunita, S.; Takahashi, S.; Wismans, R. G. P.; van Kuppevelt, T. H.; Masu, M.; Keino-Masu, K. *J. Biol. Chem.* **2012**, *287*, 9579−9590.
(40) Warda, M.; Toida, T.; Zhang, F. M.; Sun, P. L.; Munoz, E.; Xie, J.; Linhardt, R. J. *Glycoconjugate J.* **2006**, *23*, 555−563.
(41) Lee, A.; Chick, J. M.; Kolarich, D.; Haynes, P. A.; Robertson, G. R.; Tsoli, M.; Jankova, L.; Clarke, S. J.; Packer, N. H.; Baker, M. S. *Mol. Cell. Proteomics* **2011**, DOI: 10.1074/mcp.M900538-MCP200.
(42) Taraslia, V. K.; Kouskoukis, A.; Anagnostopoulos, A. K.; Stravopodis, D. J.; Margaritis, L. H.; Tsangaris, G. T. *Cancer Genomics Proteomics* **2013**, *10*, 125−54.
(43) Shi, R.; Kumar, C.; Zougman, A.; Zhang, Y.; Podtelejnikov, A.; Cox, J.; Wisniewski, J. R.; Mann, M. *J. Proteome Res.* **2007**, *6*, 2963−2972.
(44) Lai, K. K. Y.; Kolippakkam, D.; Beretta, L. *Hepatology* **2008**, *47*, 1043−1051.
(45) Lawrence, R.; Lu, H.; Rosenberg, R. D.; Esko, J. D.; Zhang, L. *Nat. Methods* **2008**, *5*, 291−292.